processes

MDPI

Article

# Research on the Characteristics of Mismatch Horizontal Deformation in Primary Coal-Rock Combination

**Qiang Fu [1,2], Taotao Du [1,2], Yongbo Cai [3,4,5,6,*], Chao Xu [6], Zihan Qin [1,2], Ruda Sun [1,2] and Ruibing Yan [7]**

[1] Coal Mining and Designing Department, CCTEG—Coal Mining Research Institute, Beijing 100013, China
[2] Tiandi Science and Technology Co., Ltd., Beijing 100013, China
[3] Emergency Science Research Academy, Chinese Institute of Coal Science, Beijing 100013, China
[4] Joint National-Local Engineering Research Centre for Safe and Precise Coal Mining, Anhui University of Science and Technology, Huainan 232001, China
[5] China Coal Research Institute, Beijing 100013, China
[6] School of Emergency Management and Safety Engineering, China University of Mining & Technology (Beijing), Beijing 100083, China
[7] Xinjiang Energy and Chemical Industry Co., Ltd., CHN Energy, Urumqi 830027, China
* Correspondence: caiyongbo0328@126.com

**Abstract**

The essence of coal-rock dynamic disasters is the instantaneous instability that occurs when the coal-rock combination system reaches its strength limit. The differing mechanical properties of coal and rock lead to mismatching deformation within the combination, thereby altering the mechanical characteristics of the coal-rock body under combination structures. Consequently, studying the mismatching horizontal deformation of coal-rock combinations is significant for the prevention and control of coal-rock dynamic disasters. To investigate the mismatching horizontal deformation characteristics of primary coal-rock combinations, this study conducted uniaxial and conventional triaxial loading experiments on primary coal-rock combinations to obtain their strength and horizontal deformation characteristics. Subsequently, numerical simulations were performed to analyze the factors influencing the horizontal deformation of primary coal-rock combinations, ultimately leading to the construction of a horizontal deformation distribution model for primary coal-rock combinations. The research results indicate that due to the influence of the coal-rock interface, the primary coal-rock combinations exhibit continuous and smooth mismatching horizontal deformation under loading conditions, with the magnitude of deformation ordered as coal > interface > rock. The influence of the interface on the horizontal deformation of the coal-rock body does not suddenly vanish; rather, it gradually diminishes with increasing distance from the interface, becoming negligible at approximately 48% of the model's lateral dimensions. A horizontal deformation mismatch distribution model for primary coal-rock combinations was established based on the Sigmoid function, and the key parameter *b* in the model was obtained through fitting with numerical simulation results. The reliability of the model was subsequently validated through experimental results. The findings of this study provide a basis for further research on the mechanical properties and deformation characteristics of coal-rock combinations.

**Keywords:** primary coal-rock combinations; coal-rock height ratio; horizontal deformation mismatch; triaxial loading

Check for updates

Academic Editor: Reza Taherdangkoo

Received: 12 May 2026
Revised: 11 June 2026
Accepted: 26 June 2026
Published: 28 June 2026

## 1. Introduction

Coal is a crucial fundamental energy source and industrial raw material in China. With the increasing demand for coal, Chinese coal mines are progressively entering deep mining, where the complex mining environment exacerbates the severity of dynamic disasters in coal-rock systems [1–4]. In addition to external conditions such as mining-induced stress and gas pressure, the mechanical and deformation characteristics of coal-rock materials are significant factors influencing dynamic disasters in coal-rock systems [5–7]. As a typical sedimentary rock, coal exhibits a layered structure, which is its most distinctive characteristic. Influenced by sedimentary environments and subsequent tectonic actions, layered coal-rock formations present varying proportions, angles, and interface structures. The mechanical characteristics of coal-rock combinations can vary significantly depending on their structural configurations. Therefore, the structural characteristics of coal-rock formations are important factors affecting dynamic disasters in coal-rock systems [8,9], and understanding the mechanical characteristics of coal-rock combinations is crucial for the prevention and control of these disasters.

Domestic and international researchers have conducted extensive studies on coal-rock combinations, concluding that the mechanical properties of these combinations are influenced by the mechanical properties of individual coal and rock units and the structural configuration of the combination [10–12]. Failure in horizontally layered coal-rock combinations is primarily due to the failure of the coal body, with the strength of the combination being greater than that of the coal but less than that of the rock [8,13–15]. Some scholars have investigated horizontal-interface coal-rock combinations with different layer orders (e.g., coal-rock, rock-coal-rock, coal-rock-coal) and height ratios, discovering that regardless of the combination type, the strength of the combination decreases as the proportion of coal increases [16–20]. Additionally, some researchers have studied coal-rock combinations with varying interface angles, finding that the combination strength diminishes with increasing interface angle, transitioning from dominant coal body failure to predominant interface slip failure [21–25]. Due to the difficulties in sampling and processing primary coal-rock combinations, many experimental studies on coal-rock combinations typically involve first processing small-sized, smooth-interface coal and rock units and subsequently assembling or bonding them to create specimens that meet experimental size requirements. This approach fails to preserve the original interface structure of the primary coal-rock combination, resulting in discrepancies in the cohesive strength of the interface compared with actual conditions.

Research on coal-rock combinations indicates that since coal's elastic modulus is generally lower than that of rock but its Poisson's ratio is higher, the horizontal deformation of the coal body under load is greater than that of the rock [26–28]. In loaded coal-rock combinations due to the interconnection at the interface, the deformation of the coal and rock at the interface remains uniform. Compared with individual coal and rock units, the coal body is constrained at the interface, while the rock expands, generating horizontal compressive stress in the coal body and tensile stress in the rock. This results in an increase in the coal's strength while reducing the rock's strength [14,27,29,30]. The existence of mismatching horizontal deformation serves as a foundational theoretical framework for current research on the mechanical and damage characteristics of coal-rock combinations. However, there is limited research on the extent of constraint exerted by coal-rock interfaces. Most studies on mismatching horizontal deformation in coal-rock systems analyze coal-rock bodies adjacent to the interface separately from those farther away. For coal-rock combinations with cohesive forces, the horizontal deformation should be continuous and smooth due to the constraints of the interface [31]. Thus, there are some deficiencies in the research on mismatching horizontal deformation in coal-rock combinations.

https://doi.org/10.3390/pr14132100

In response to these deficiencies, this study utilized large blocks of coal-rock combination materials to fabricate primary coal-rock combinations with different height ratios. Uniaxial and triaxial loading experiments were conducted using an MTS electronic universal testing machine and an RTX-3000 rock triaxial testing system, respectively, to obtain the strength and horizontal deformation characteristics of the coal-rock combinations. Through numerical simulation, the effects of various factors on the horizontal deformation of the coal-rock combinations were analyzed. Ultimately, a horizontal deformation mismatch distribution model for primary coal-rock combinations was constructed based on the Sigmoid function. The findings of this study provide a significant basis for further research on the mechanical properties and deformation characteristics of coal-rock combinations.

## 2. Experimental Study on the Characteristics of Mismatching Horizontal Deformation in Primary Coal-Rock Combinations

Primary coal-rock combination specimens with different coal-rock height ratios were prepared, and conventional triaxial loading experiments were conducted using the RTX-3000 rock triaxial testing system (GCTS Testing Systems, Inc., Tempe, AZ, USA) and MTS-e45.305 electronic universal testing machine (MTS Systems Corporation, Eden Prairie, MN, USA). This allowed us to obtain the strength and horizontal deformation characteristics of primary coal-rock combinations at varying coal-rock height ratios.

### 2.1. Specimen Preparation

The specimens selected for this study were all sourced from coal seam #8 of the Shendong Baode Coal Mine. The thickness of coal seam #8 ranges from 3.83 to 10.39 m, with an average of 7.46 m. Its net coal thickness varies between 3.19 and 8.84 m, averaging 6.01 m. This coal seam is classified as a medium-thick to extra-thick coal seam, dominated by a thick coal seam. The coal seam contains 3 to 9 partings, generally 3 to 4 partings. The total thickness of the partings is 0.3 to 2.6 m, with an average of 1.06 m, and the maximum thickness of a single parting is 0.65 m. Lithologically, the partings are mainly mudstone, followed by carbonaceous mudstone.

Large blocks of coal-rock samples, byproducts of the tunneling process, were processed using numerical-control wire cutting technology to create primary coal-rock combinations with dimensions of φ50 mm and h100 mm, at coal-rock height ratios of 5:5, 6:4, 7:3, 8:2, and 9:1. Additionally, artificial coal-rock combinations with a height ratio of 5:5, as well as coal and rock specimens, were prepared for uniaxial and triaxial loading experiments (Figure 1).

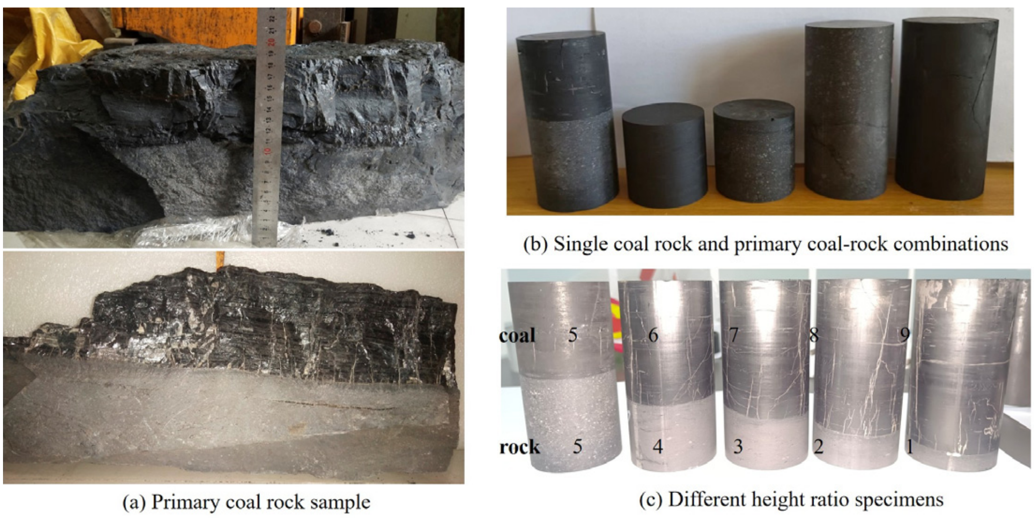


**Figure 1.** Samples of primary coal-rock combinations and different height ratios.

https://doi.org/10.3390/pr14132100

## 2.2. Experimental Equipment and Procedure

Two sets of experiments were conducted: uniaxial and triaxial loading. The uniaxial loading experiments were accompanied by digital image correlation (DIC) deformation experiments, focusing on primary coal-rock combinations with a height ratio of 5:5, artificial coal-rock combinations with the same height ratio, and coal and rock specimens. The uniaxial loading system used was an MTS-e45.305 electronic universal testing machine with a maximum load capacity of 300 kN, and the deformation monitoring system was the ISM-2D system produced by IMETRUM in the Bristol, UK (Figure 2a). Prior to the experiments, a layer of black paint was uniformly sprayed on the front surface of each specimen, which was then allowed to dry before a layer of white paint was applied to create a random artificial speckle field, serving as the carrier for deformation information (Figure 2b). After the formation of the digital speckle pattern was confirmed, the combination specimens were positioned between the upper and lower pressure plates of the testing machine, with the rock layer on the bottom and the coal layer on the top. The digital image acquisition equipment was installed and adjusted to ensure that high-quality digital images could be collected. Image acquisition commenced while loading was performed at a constant displacement rate of 0.1 mm/min, during which digital speckle images of the specimen's front surface were continuously collected. At the conclusion of the experiment, image acquisition was stopped, and the speckle images were imported into digital image correlation software to compute the deformation field during the loading process. Due to the high strength of the primary rock, the energy released during its failure was substantial, posing a risk of damage to the imaging equipment. Therefore, two sets of tests were performed on the primary rock: in the first set, the rock was loaded to 70 MPa and then unloaded to capture the deformation field, while in the second set, after the equipment was removed and a protective cover was added, the rock was loaded to failure to obtain the strength and failure characteristics.

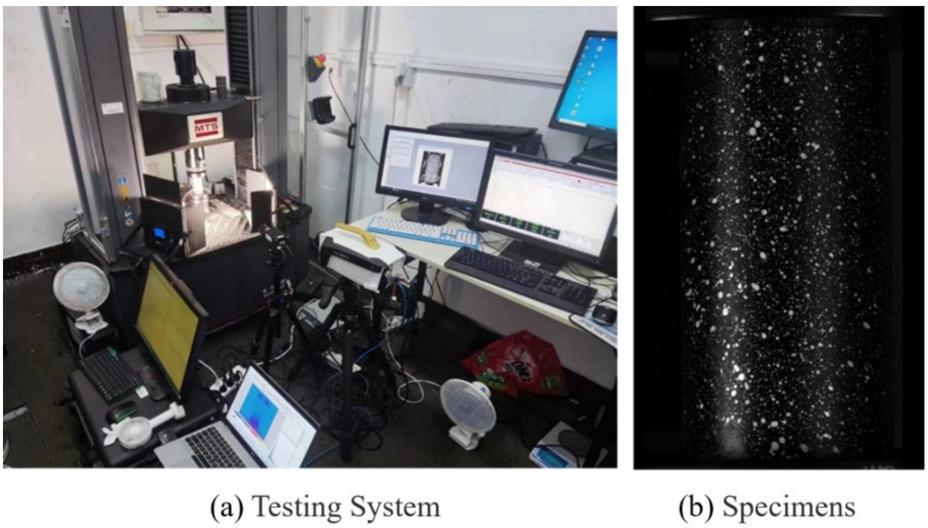


**Figure 2.** DIC testing system and sample.

The triaxial loading subjects included primary coal-rock combinations with height ratios of 5:5, 6:4, 7:3, 8:2, and 9:1, as well as coal specimens. The experimental testing system employed was the RTX-3000 rock triaxial testing system produced by GCTS, USA (Figure 3a). In this experiment, the specimens were arranged with the rock portion positioned below, utilizing a fixed confining pressure ($\sigma_2$) of 8 MPa, and axial pressure ($\sigma_1$) was applied until specimen failure occurred in a triaxial loading configuration. During the loading process, a chain-type circumferential extensometer was used to measure the

https://doi.org/10.3390/pr14132100

horizontal deformation of the specimens. The circumferential extensometers were installed at the center of each specimen (Figure 2b). Due to the differing height ratios of the coal-rock specimens, with other conditions kept constant, it was possible to measure the horizontal deformations of the primary coal-rock combination specimens at distances of 0, 1, 2, 3, and 4 cm from the coal-rock interface, as well as the horizontal deformation of the coal body in the coal specimens, which is assumed to be equivalent to the horizontal deformation of the coal body at an infinite distance from the interface [27].

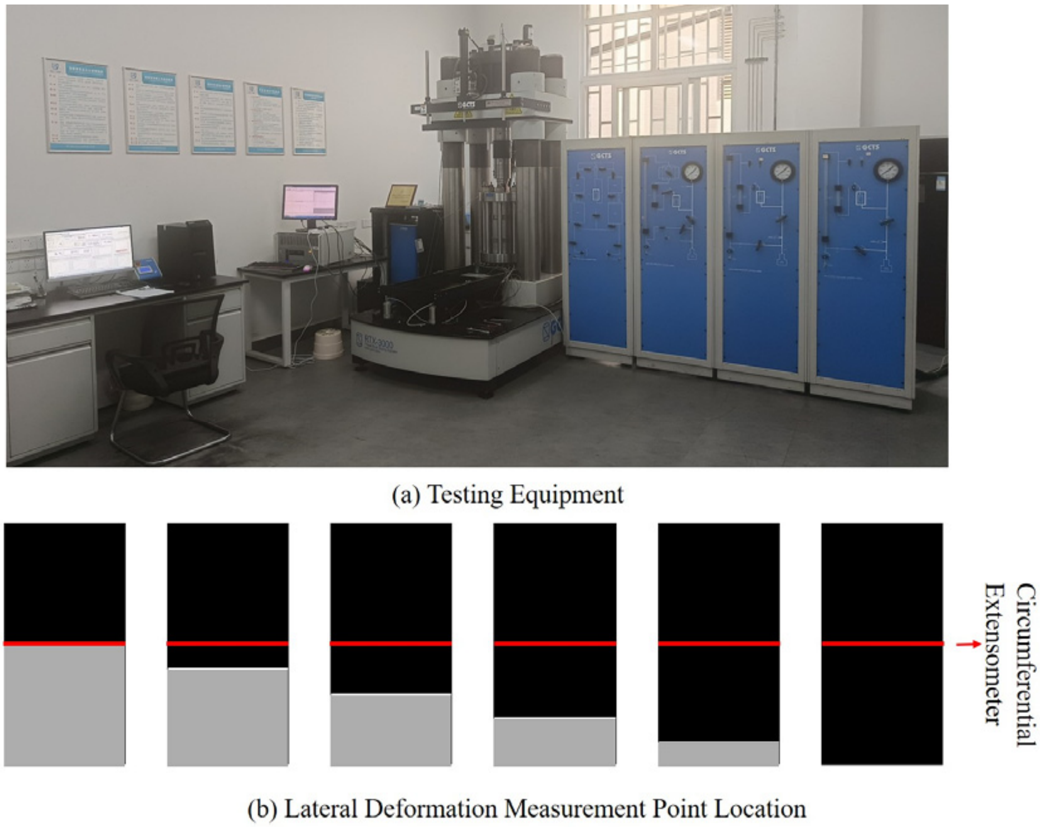


**Figure 3.** Uniaxial test equipment and measurement points.

## 2.3. Experimental Results

### 2.3.1. Uniaxial Test Results

(1) Strength Characteristics

The axial stress–strain curves of the primary rock, primary coal, primary coal-rock combinations, and artificial coal-rock combinations under uniaxial loading conditions are shown in Figure 4. The uniaxial strengths of the primary rock, primary coal, primary coal-rock combinations, and artificial coal-rock combinations were 91.40, 15.21, 30.24, and 42.18 MPa, respectively. The strength of the primary rock was significantly greater than that of the other specimens, while the primary coal exhibited the lowest strength, with the strengths of the two combination types falling between those of the primary rock and coal.

(2) Horizontal Deformation Characteristics

During the experiments, due to severe surface damage to the primary coal specimens, effective data could not be collected using DIC. Therefore, only the horizontal deformation characteristics of the primary rock, primary coal-rock combinations, and artificial coal-rock combinations were analyzed. The horizontal displacement contour maps for the three specimens are shown in Figures 5–7.

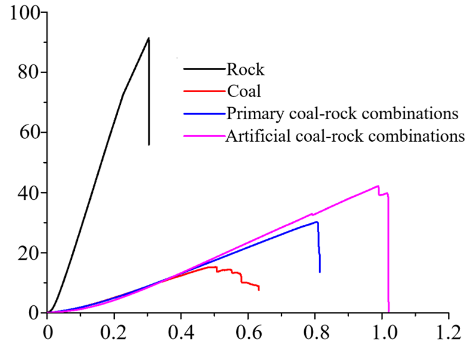


**Figure 4.** Relationship between axial stress and strain.

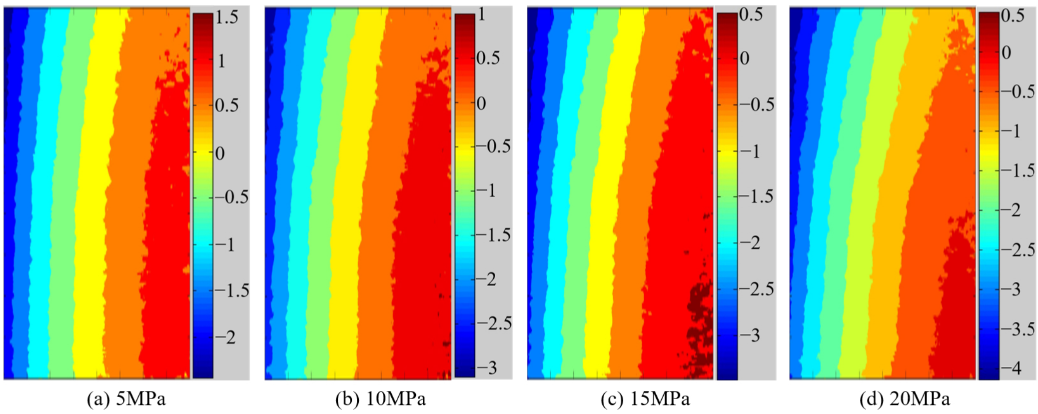


**Figure 5.** Horizontal displacement contours of rock.

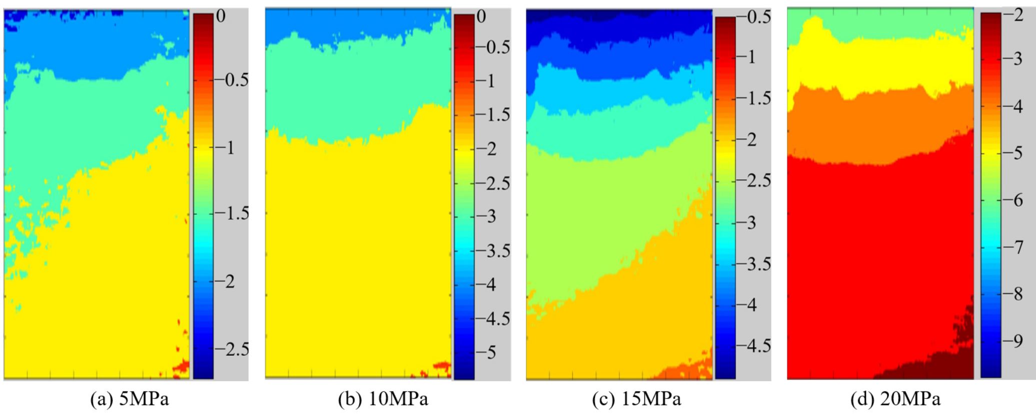


**Figure 6.** Horizontal displacement contours of primary coal-rock combination.

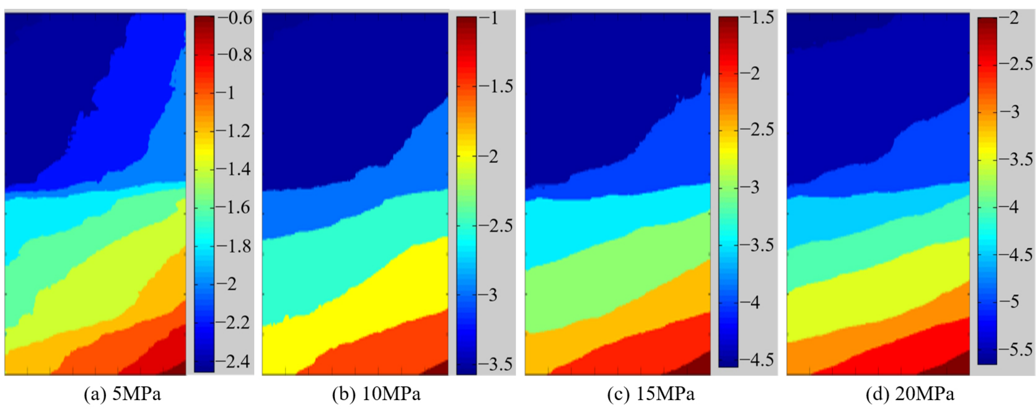


**Figure 7.** Horizontal displacement contours of artificial coal-rock combination.

From the figures, it can be observed that the horizontal deformation of the primary rock was uniformly distributed, with deformation at various positions along the vertical direction being nearly identical. In contrast, the deformation of the coal sections in the primary coal-rock and artificial coal-rock combinations was significantly greater than that of the primary rock. The distribution of horizontal deformation at the edges of the specimens under different stress conditions is illustrated in Figure 8.

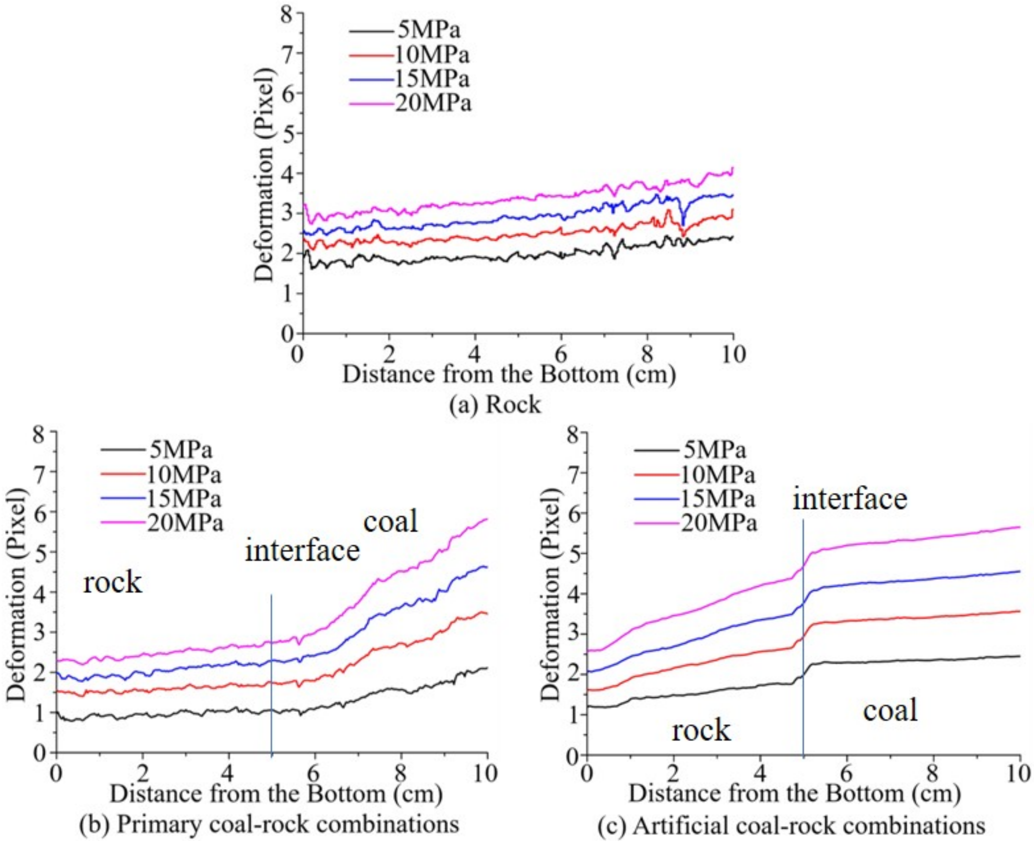


**Figure 8.** Horizontal deformation distribution under different axial pressures.

The horizontal deformation at various positions in the rock, artificial coal-rock combinations, and primary coal-rock combinations increased with an increase in axial pressure, following the order coal > interface > rock in both coal-rock combination specimens. At the same axial pressure, the horizontal deformation of the primary rock specimen fluctuated within a certain range, maintaining a general uniformity across positions. However, for the primary coal-rock combination specimens, the horizontal deformation distribution in the primary rock portion remained relatively uniform (horizontal coordinates 0–5 cm), while near the coal-rock interface (at the horizontal coordinate of 5 cm), it gradually increased with depth into the coal body, indicating a smooth transition in the horizontal deformation distribution between the coal and rock bodies at the interface. The horizontal deformation of the coal body and rock body in the artificial coal-rock combinations varied markedly, with the horizontal deformation at the coal-rock interface (at the horizontal coordinate of 5 cm) exhibiting a pronounced jump. Due to the lower elastic modulus and higher Poisson's ratio of the coal body, the horizontal deformation of the coal body exceeds that of the rock body under the same loading conditions. The fundamental reason for the differences in the horizontal deformation distribution at the interface in the primary coal-rock combinations and artificial coal-rock combinations lie in the varying inter-layer interactions. The primary coal-rock combinations maintain no relative displacement in the horizontal direction due to the presence of inter-layer cohesion, while the artificial coal-rock combinations lack adhesive treatment between the layers, causing relative displacement at the coal-rock interface when frictional forces are insufficient to constrain the deformation of the coal body, leading to sharp changes in horizontal deformation near the interface. In deep mining coal seams that have not been disturbed by excavation or have experienced minimal disturbance, the coal-rock interface is often resistant to failure, with the coal-rock body forming a combination due to cohesive forces at the interface.

### 2.3.2. Triaxial Test Results

The differential stress–strain curves during the loading process for primary coal-rock combinations with varying coal-rock height ratios are shown in Figure 9.

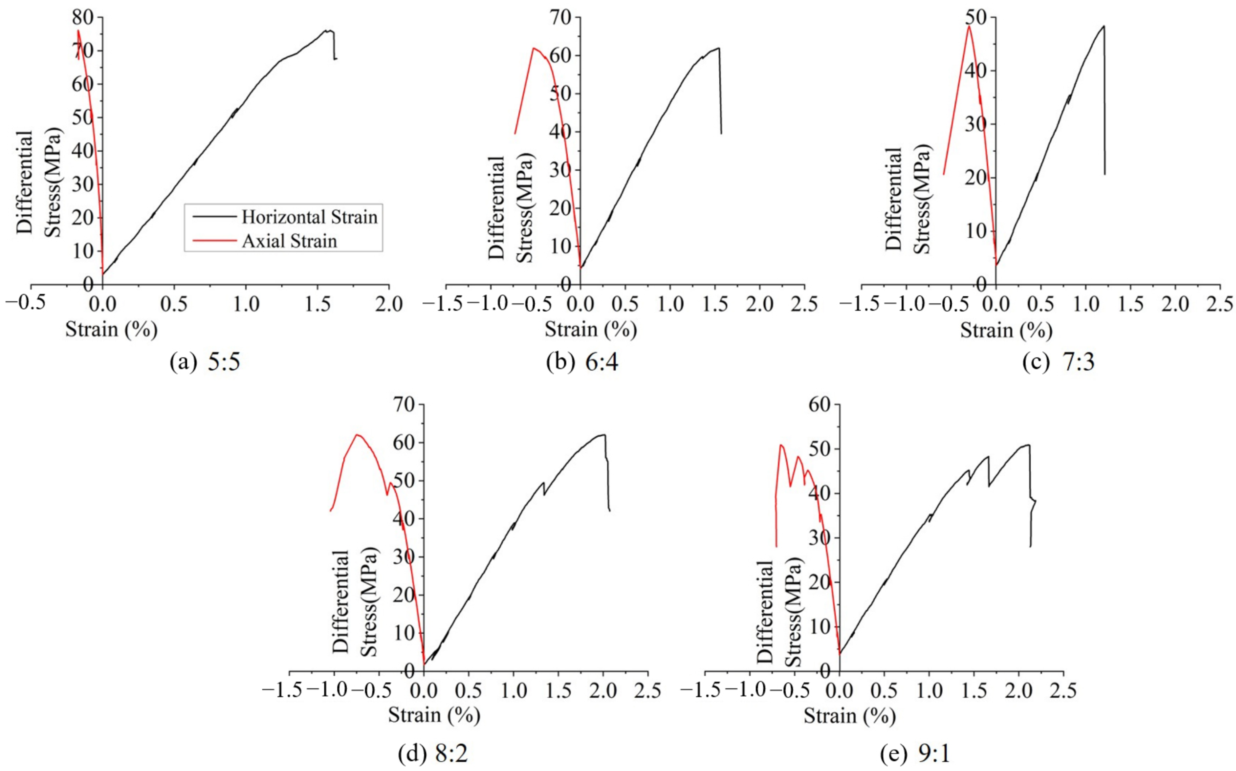


**Figure 9.** Relationship between deviatoric stress and strain of primary coal-rock combinations with different coal-rock height ratios.

The peak differential stresses during the loading of primary coal-rock combinations with height ratios of 5:5, 6:4, 7:3, 8:2, and 9:1 were 75.1, 61.9, 48.4, 62.1, and 50.9 MPa, respectively, corresponding to axial strains of 1.5245%, 1.552%, 1.1941%, 1.9182%, and 1.8164%, as well as horizontal strains of −0.1166%, −0.5966%, −0.3021%, −1.1049%, and −0.6487%. Overall, the strength of the primary coal-rock combination specimens decreased with increasing coal-rock height ratio, with the specimen at a height ratio of 8:2 exhibiting relatively high strength. This may be attributed to the fact that, although all specimens were prepared from the same large sample, it was not possible during processing to control the number and size of randomly distributed cracks within the coal-rock material. The primary coal-rock combination specimen with a height ratio of 8:2 likely contained fewer internal cracks, resulting in higher strength. The horizontal strain of the coal body during the elastic stage at different positions within the primary coal-rock combination under the same differential stress is shown in Figure 10.

https://doi.org/10.3390/pr14132100

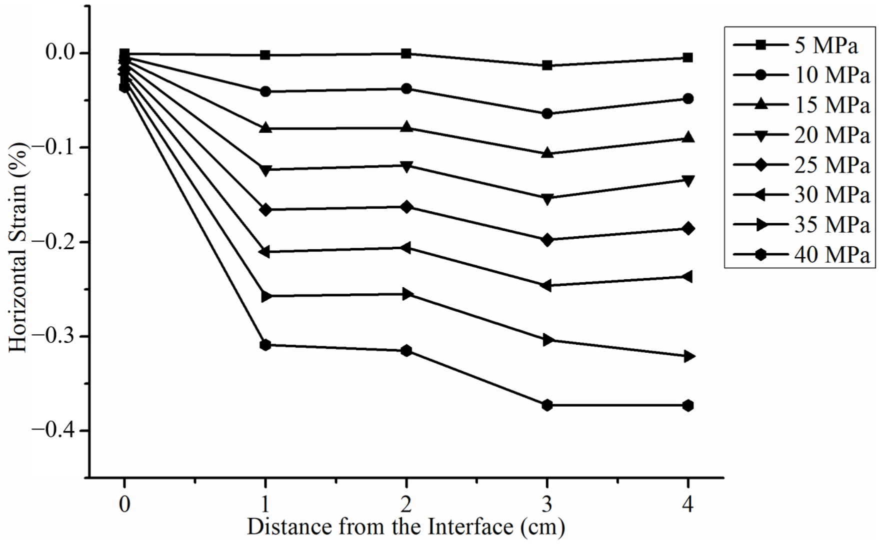


**Figure 10.** Horizontal strain of the coal at different positions from the interface in the primary coal-rock combination.

Figure 10 shows that the horizontal strain at the coal-rock interface was minimal. As the distance from the interface increased, the horizontal strain of the coal body in the primary coal-rock combination gradually increased, albeit at a decreasing rate, stabilizing at a distance of 3 cm from the interface. The deformation generated by the constraint at the interface can be equivalently described as the deformation induced by the derived stresses at the interface, which represents a balanced force system. According to Saint-Venant's principle, if a small portion of an elastic body (in area or volume) experiences a balanced force system, this load primarily induces significant stress in the nearby local region, while the stress at a distance can be neglected. Consequently, the interface's constraint on the coal body's deformation only affects the local area, with the deformation of coal bodies farther from the interface remaining unaffected by its constraints.

## 3. Numerical Simulation Study on the Characteristics of Mismatching Horizontal Deformation in Coal-Rock Combinations

To investigate the influencing factors of mismatching horizontal deformation in primary coal-rock combinations, FLAC 3D (5.0) numerical simulation software was utilized to obtain the distribution characteristics of horizontal deformation under various mechanical parameters, stress states, and specimen dimensions.

### *3.1. Numerical Simulation Model and Scheme*

The simulation model was a cubic structure with dimensions of 1:1:2 (x:y:z) and a mesh count of 25:25:50 (x:y:z), employing an elastic model. Stress boundaries were applied at the top and around the model, while a fixed boundary was set at the bottom. During the experiment, the expansion deformation of the coal body due to gas adsorption could also be considered as deformation caused by changes in the mechanical parameters of the coal-rock system; therefore, the simulation did not account for expansion deformation caused by gas adsorption. After the equilibrium under predetermined conditions was calculated, the displacements of the midline nodes on the model's side were output. The specific mechanical parameters and stress states for each simulation are shown in Table 1.

https://doi.org/10.3390/pr14132100

**Table 1.** Numerical simulation scheme.

| No. | Coal Elastic Modulus (GPa) | Rock Elastic Modulus (GPa) | Coal Poisson's Ratio | Rock Poisson's Ratio | Model Size | Axial Pressure | Confining Pressure |
|---|---|---|---|---|---|---|---|
| 1 | 6 | 11 | 0.3 | 0.2 | 5 cm × 5 cm × 10 cm | 10 | 0 |
| 2 | 7 | 11 | 0.3 | 0.2 | 5 cm × 5 cm × 10 cm | 10 | 0 |
| 3 | 8 | 11 | 0.3 | 0.2 | 5 cm × 5 cm × 10 cm | 10 | 0 |
| 4 | 9 | 11 | 0.3 | 0.2 | 5 cm × 5 cm × 10 cm | 10 | 0 |
| 5 | 10 | 11 | 0.3 | 0.2 | 5 cm × 5 cm × 10 cm | 10 | 0 |
| 6 | 10 | 12 | 0.3 | 0.2 | 5 cm × 5 cm × 10 cm | 10 | 0 |
| 7 | 10 | 13 | 0.3 | 0.2 | 5 cm × 5 cm × 10 cm | 10 | 0 |
| 8 | 10 | 14 | 0.3 | 0.2 | 5 cm × 5 cm × 10 cm | 10 | 0 |
| 9 | 10 | 15 | 0.3 | 0.2 | 5 cm × 5 cm × 10 cm | 10 | 0 |
| 10 | 10 | 15 | 0.32 | 0.2 | 5 cm × 5 cm × 10 cm | 10 | 0 |
| 11 | 10 | 15 | 0.34 | 0.2 | 5 cm × 5 cm × 10 cm | 10 | 0 |
| 12 | 10 | 15 | 0.36 | 0.2 | 5 cm × 5 cm × 10 cm | 10 | 0 |
| 13 | 10 | 15 | 0.38 | 0.2 | 5 cm × 5 cm × 10 cm | 10 | 0 |
| 14 | 10 | 15 | 0.3 | 0.22 | 5 cm × 5 cm × 10 cm | 10 | 0 |
| 15 | 10 | 15 | 0.3 | 0.24 | 5 cm × 5 cm × 10 cm | 10 | 0 |
| 16 | 10 | 15 | 0.3 | 0.26 | 5 cm × 5 cm × 10 cm | 10 | 0 |
| 17 | 10 | 15 | 0.3 | 0.28 | 5 cm × 5 cm × 10 cm | 10 | 0 |
| 18 | 10 | 15 | 0.3 | 0.2 | 5 cm × 5 cm × 10 cm | 2 | 0 |
| 19 | 10 | 15 | 0.3 | 0.2 | 5 cm × 5 cm × 10 cm | 4 | 0 |
| 20 | 10 | 15 | 0.3 | 0.2 | 5 cm × 5 cm × 10 cm | 6 | 0 |
| 21 | 10 | 15 | 0.3 | 0.2 | 5 cm × 5 cm × 10 cm | 8 | 0 |
| 22 | 10 | 15 | 0.3 | 0.2 | 5 cm × 5 cm × 10 cm | 10 | 2 |
| 23 | 10 | 15 | 0.3 | 0.2 | 5 cm × 5 cm × 10 cm | 10 | 4 |
| 24 | 10 | 15 | 0.3 | 0.2 | 5 cm × 5 cm × 10 cm | 10 | 6 |
| 25 | 10 | 15 | 0.3 | 0.2 | 5 cm × 5 cm × 10 cm | 10 | 8 |
| 26 | 10 | 15 | 0.3 | 0.2 | 10 cm × 10 cm × 20 cm | 10 | 0 |
| 27 | 10 | 15 | 0.3 | 0.2 | 20 cm × 20 cm × 40 cm | 10 | 0 |
| 28 | 10 | 15 | 0.3 | 0.2 | 40 cm × 40 cm × 80 cm | 10 | 0 |
| 29 | 10 | 15 | 0.3 | 0.2 | 80 cm × 80 cm × 160 cm | 10 | 0 |

### *3.2. Characteristics of Horizontal Deformation Distribution*

When loaded, the axial and lateral deformations of the coal-rock combinations are far smaller than the original dimensions of the specimen. Therefore, in analyzing the distribution of horizontal deformation in the coal-rock combination, the axial deformation during loading is ignored. The influence of various elastic moduli of coal and rock on the lateral deformation of coal-rock combinations is illustrated in Figure 11, where the horizontal coordinate zero indicates the interface position.

Figure 11 shows that under the same axial pressure, variations in the elastic moduli of coal and rock affect not only their own deformation but also the deformation of the interface. In the combination, while the elastic modulus of another part remains fixed, a decrease in the elastic modulus of coal or rock leads to a corresponding decrease in their deformation and that of the interface. For coal, as the distance from the interface increases, its deformation gradually increases, albeit at a decreasing rate, stabilizing after a distance greater than 0.024 m. For rock, the deformation decreases as the distance from the interface increases, also at a decreasing rate, and remains nearly unchanged beyond a distance of 0.02 m. The effects of different Poisson's ratios of coal and rock on the lateral deformation of coal-rock combinations are shown in Figure 12.

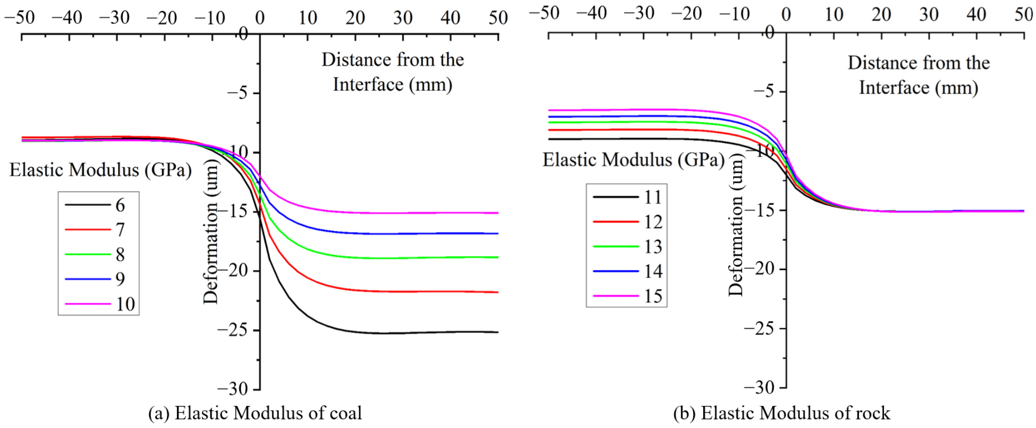


**Figure 11.** Effect of elastic moduli of coal and rock on horizontal deformation.

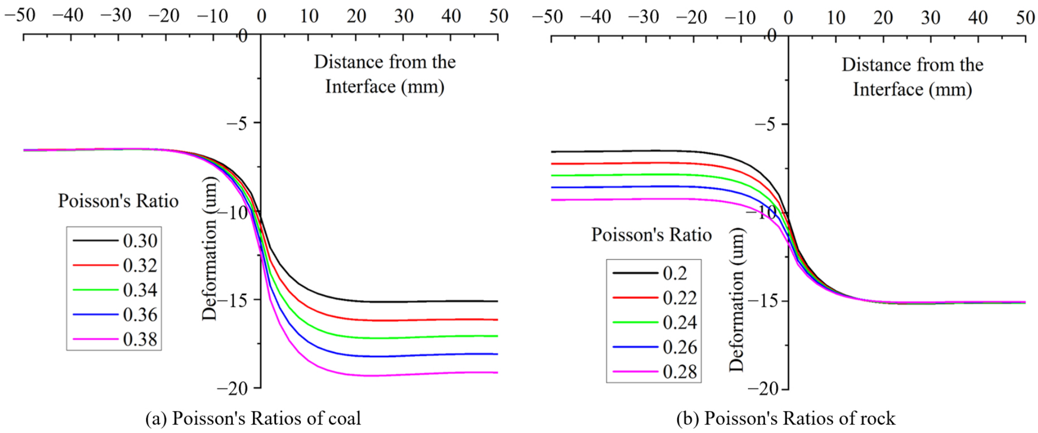


**Figure 12.** Effect of Poisson's ratio of coal and rock on horizontal deformation.

Figure 12 shows that similarly to the impact of the elastic modulus on horizontal deformation, changes in the Poisson's ratios of coal and rock under the same axial pressure affect their own deformations and that of the interface. However, in the combination, while the Poisson's ratio of another part remains fixed, an increase in the Poisson's ratio of coal or rock leads to an increase in their deformation and that of the interface. For coal, as the distance from the interface increases, its deformation gradually increases but at a decreasing rate, stabilizing beyond a distance greater than 0.024 m. For rock, the deformation gradually decreases with increasing distance from the interface, also at a decreasing rate, remaining nearly unchanged beyond a distance greater than 0.024 m. The influence of axial pressure and confining pressure on the horizontal deformation of coal-rock combinations is illustrated in Figure 13.

Figure 13 shows that the horizontal deformation at various positions within the coal-rock combination increases with increasing axial pressure. Calculations indicate that the horizontal deformation at each position has a direct proportional relationship with the axial pressure. As confining pressure increases, the horizontal deformation at various locations within the combination gradually decreases, transitioning from expansion deformation to compression deformation. Under a confining pressure of 4 MPa, the coal in the combination exhibits expansion deformation, while the rock exhibits compression deformation, although the dimensions of the coal remain greater than those of the rock. For coal, as the distance from the interface increases, its deformation gradually increases but at a decreasing rate, stabilizing beyond a distance greater than 0.024 m. For rock, as the distance from the interface increases, the deformation gradually decreases but at a decreasing rate, stabilizing beyond a distance greater than 0.024 m. The influence of model size on the deformation of coal-rock combinations is shown in Figure 14.

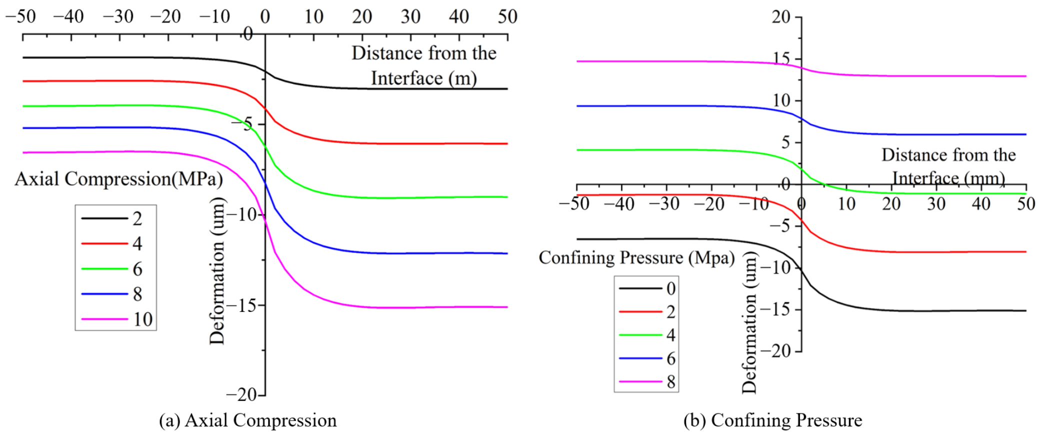


**Figure 13.** Effect of axial pressure and confining pressure on horizontal deformation.

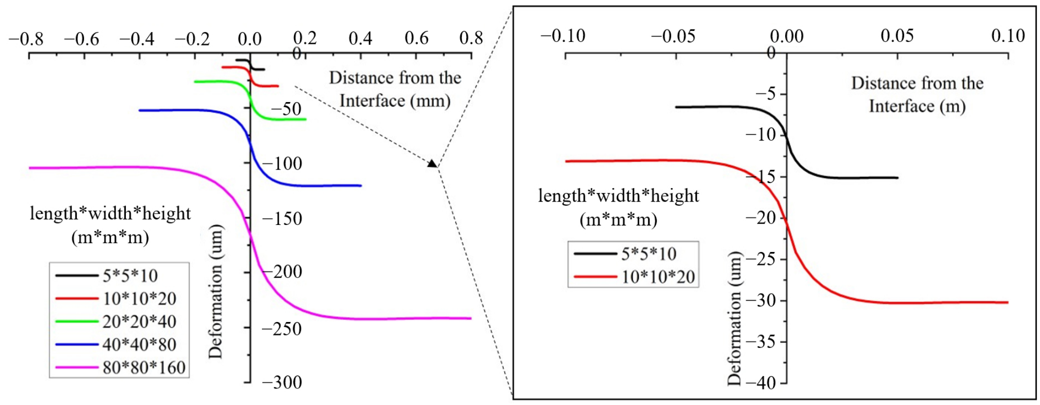


**Figure 14.** Effect of the size of coal-rock combination on horizontal deformation.

From Figure 14, it is clear that there are significant differences in horizontal deformation and deformation distributions between coal-rock combinations of varying sizes. In the five groups of simulations, the maximum deformations of coal were $1.51 \times 10^{-5}$, $3.02 \times 10^{-5}$, $6.04 \times 10^{-5}$, $1.21 \times 10^{-4}$, and $2.42 \times 10^{-4}$ m; the interface deformations were $1.04 \times 10^{-5}$, $2.07 \times 10^{-5}$, $4.14 \times 10^{-5}$, $8.28 \times 10^{-5}$, and $1.65 \times 10^{-4}$ m; and the maximum deformations of rock were $6.55 \times 10^{-6}$, $1.31 \times 10^{-5}$, $2.62 \times 10^{-5}$, $5.24 \times 10^{-5}$, and $1.05 \times 10^{-4}$ m, with the deformations of coal, rock, and the interface increasing proportionally with the model's lateral dimensions. The convergence of coal and rock occurred at fixed values at distances of 0.0288, 0.058, 0.115, 0.230, and 0.460 m, with an influence range of approximately 0.48 times the model's lateral dimensions.

From the experiments and numerical simulations, it is evident that regardless of varying conditions, the lateral dimensions of the coal-rock combination follow the order coal > interface > rock. The deformation of the coal-rock body remains virtually unchanged beyond a distance approximately 48% greater than the model's lateral dimensions, where horizontal deformation equals that of coal or rock. The impact of the interface on horizontal deformation in coal-rock combinations does not abruptly vanish; rather, it gradually diminishes to a negligible level for coal or rock that is farther from the interface.

## 4. Horizontal Stress–Strain Distribution Model of Primary Coal-Rock Combinations

Based on the triaxial loading test results for primary coal-rock combinations with different height ratios, the deformation distribution test results using DIC technology, and numerical simulation calculations, it was observed that the horizontal deformation distribution in primary coal-rock combinations is continuous and smooth. As the distance from the interface increases, the deformation gradually converges to that of the original coal or rock, exhibiting an "S"-shaped distribution. A model for the horizontal deformation mismatch of primary coal-rock combinations was established based on the Sigmoid function, leading to the derivation of the horizontal stress distribution model for these combinations.

### 4.1. Horizontal Strain Distribution Model

Under the influence of the interface, the horizontal strain distribution of primary coal-rock combinations closely resembles the arctangent function and the Sigmoid function (Equation (1)). However, since the Sigmoid function has a simpler structure and is easier to differentiate or integrate, it is more suitable for subsequent research based on this model. Therefore, the Sigmoid function was chosen as the foundational function for the model:

$$\mathrm{S(x) = 1/(1 + e - x)} \tag{1}$$

Letting the horizontal coordinate represent the distance $H$ from the interface for various positions within the primary coal-rock combination, with the zero coordinate at the interface, the positive half-axis for coal, the negative half-axis for rock, and the vertical axis representing the horizontal strain $\varepsilon_h$ at different locations, we have the following:

When $H = 0$, $\varepsilon_h$ is the strain at the interface, $\varepsilon_{jh}$; when $H$ approaches $+\infty$, $\varepsilon_h$ is the strain of coal, $\varepsilon_{ch}$; and when $H$ approaches $-\infty$, $\varepsilon_h$ is the strain of rock, $\varepsilon_{rh}$. Additionally, as noted in Section 3.2, the influence range of the interface on the coal and rock constraints is related to the horizontal size of the interface, showing a clear and direct proportional relationship. Under conventional triaxial conditions $\sigma_2 = \sigma_{3=} = \sigma_h$, the horizontal strain $\varepsilon_h$ of the coal-rock body and the distance $H$ from the interface are related as follows:

$$\lim_{H \to -\infty} \varepsilon_{h1}(H) = \varepsilon_{rh} \tag{2}$$

$$\lim_{H \to +\infty} \varepsilon_{h1}(H) = \varepsilon_{ch} \tag{3}$$

$$\varepsilon_h(0) = \varepsilon_{jh} \tag{4}$$

Modifying the Sigmoid function to suit its application as a function for the horizontal strain distribution in coal and rock gives

$$\varepsilon_h = \frac{\varepsilon_{ch} - \varepsilon_{rh}}{1 + e^{k_x - \frac{0.05 \times bH}{D}}} + \varepsilon_{rh} \tag{5}$$

$$k_x = \ln\left(\frac{\varepsilon_{ch} - \varepsilon_{rh}}{\varepsilon_{jh} - \varepsilon_{rh}} - 1\right) \tag{6}$$

where $b$ is a dimensionless parameter controlling the influence range of interface constraints, dimensionless; $D$ is the model's horizontal dimension, in m.

The horizontal strains of coal, rock, and the interface can be calculated using the following equations [27,32]:

$$\varepsilon_{ch} = \frac{\sigma_h - \alpha_c p - \nu_c(\sigma_h - \alpha_c p + \sigma_1 - \alpha_c p)}{E_c} + \varepsilon_c^l \tag{7}$$

$$\varepsilon_{rh} = \frac{\sigma_h - \nu_r(\sigma_h - \alpha_c p + \sigma_1)}{E_r} \tag{8}$$

$$\varepsilon_{jh} = \frac{1}{E_c}[\sigma_h - \alpha_c P + \sigma_{2\mathrm{i}} - \nu_{\mathrm{c}}(\sigma_1 - \alpha_c P + \sigma_h - \alpha_c P + \sigma_{3\mathrm{i}})] + \varepsilon_c^l \tag{9}$$

$$\sigma_{2\mathrm{i}} = h_1\sigma_1 + h_3\sigma_2 + h_2\sigma_3 + h_4 \tag{10}$$

$$\sigma_{3\mathrm{i}} = h_1\sigma_1 + h_2\sigma_2 + h_3\sigma_3 + h_4 \tag{11}$$

$$h_1 = \frac{E_c v_r - E_r v_c}{E_r(1 - v_c) + E_c(1 - v_r)} \tag{12}$$

$$h_2 = \frac{2E_c E_r(v_r - v_c)}{(E_r + E_c)^2 - (E_r v_c + E_c v_r)^2} \tag{13}$$

$$h_3 = \frac{{E_r}^2(1 - {v_c}^2) - {E_c}^2(1 - {v_r}^2)}{(E_r + E_c)^2 - (E_r v_c + E_c v_r)^2} \tag{14}$$

$$h_4 = \frac{\varepsilon_{max}^l p}{p + p_\varepsilon} \times \frac{E_r E_c}{(v_r - 1)E_c + (v_c - 1)E_r} + \frac{E_c a_c(1 - 2v_c) - E_c a_r(1 - 2v_r)}{(v_r - 1)E_c + (v_c - 1)E_r} p \tag{15}$$

$$\varepsilon_{\mathrm{c}}^l = -\frac{\varepsilon_{\mathrm{max}}^l p}{p + p_\varepsilon} \tag{16}$$

where $E_r$ is the elastic modulus of the rock, in GPa; $\nu_r$ is the Poisson's ratio of the rock, dimensionless; $E_c$ is the elastic modulus of the coal, in GPa; $\nu_{\mathrm{c}}$ is the Poisson's ratio of the coal, dimensionless; $\varepsilon_{max}^l$ is the maximum volume strain of gas adsorption in the coal matrix, as a percentage; $p_\varepsilon$ is the Langmuir pressure for adsorption-induced deformation in the coal matrix, in MPa; $\alpha_c$ is the effective stress coefficient of the coal, dimensionless; $p$ is the pore pressure in the coal, in MPa.

Although the actual physical meaning of parameter $b$ cannot be clearly defined in the current study, its values fitted from numerical calculations (Table 2) show a maximum of 329.1, a minimum of 307.7, and an average of 318.5. The range of parameter $b$ is 21.4, and the relative deviations of the extreme values from the average are merely 3.33% and 3.39%, indicating slight fluctuation. Therefore, the average value of $b$ = 318.5 was adopted as the actual value, which could then be substituted into the equation to obtain the horizontal strain distribution model for coal-rock combinations, as shown in Equation (17):

$$\varepsilon_h = \frac{\varepsilon_{ch} - \varepsilon_{rh}}{1 + e^{k_x - \frac{15.9 \times H}{D}}} + \varepsilon_{rh} \tag{17}$$

The strain of the coal at distance $H$ from the interface includes two components: the strain due to vertical stress $\sigma_1$ and horizontal stress $\sigma_{hc}$, and the adsorption strain.

$$\varepsilon_h = \frac{1}{E_c}[\sigma_{hc} - \alpha_c p - \nu_{\mathrm{c}}(\sigma_1 - \alpha_c p + \sigma_{hc} - \alpha_c p)] + \varepsilon_c^l \tag{18}$$

By substituting Equation (17) into Equation (18), the horizontal stress of the coal at height $H$ from the coal-rock interface can be derived as follows:

$$\sigma_{hc} = \frac{E_c\left(\frac{\varepsilon_{ch} - \varepsilon_{rh}}{1 + e^{k_x - \frac{15.9 \times H}{D}}} + \varepsilon_{rh} - \varepsilon_c^l\right) + \nu_{\mathrm{c}}\sigma_1 - (2\nu_{\mathrm{c}} - 1)\alpha_c p}{1 - \nu_{\mathrm{c}}} \tag{19}$$

**Table 2.** The values of *b* under different conditions.

| No. | *b* | No. | *b* | No. | *b* | No. | *b* |
|---|---|---|---|---|---|---|---|
| 1 | 318.7 | 9 | 310.3 | 17 | 321 | 25 | 318.7 |
| 2 | 324.8 | 10 | 316.5 | 18 | 321.9 | 26 | 328.7 |
| 3 | 311 | 11 | 316.5 | 19 | 323.2 | 27 | 318.5 |
| 4 | 312.6 | 12 | 319.6 | 20 | 329.1 | 28 | 318.3 |
| 5 | 307.7 | 13 | 322.8 | 21 | 328.7 | 29 | 314.2 |
| 6 | 307.7 | 14 | 324.4 | 22 | 315.7 | | |
| 7 | 309.4 | 15 | 326.6 | 23 | 317.3 | | |
| 8 | 311.8 | 16 | 316.5 | 24 | 313.2 | | |

### 4.2. Model Validation

Using the horizontal strain data obtained from the experiments for the coal and the interface, horizontal strain values at different positions from the interface were calculated using Equation (19). A comparison between the theoretical calculations and experimental values is shown in Figure 15.

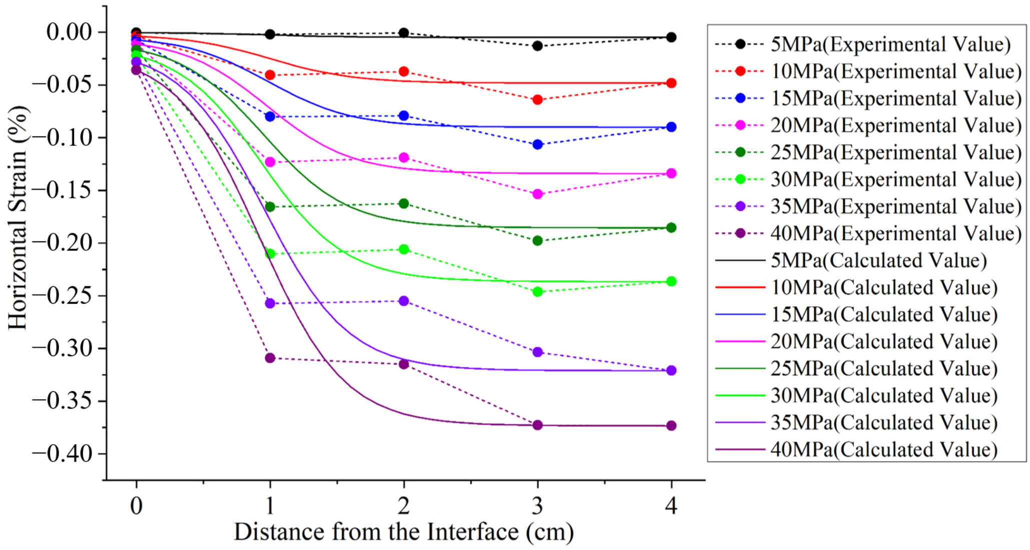


**Figure 15.** Comparison between experimental and theoretical calculated values.

At a position 2 cm from the interface, the experimentally measured horizontal strain value is lower than the theoretical calculation, which may be attributed to the heterogeneity of the specimen with a height ratio of 7:3. For other positions, the experimental values closely match the theoretical calculated values, indicating that the model proposed in this study effectively reflects the patterns of the mismatching horizontal strain distribution in primary coal-rock combinations.

## 5. Analysis of the Impact of Non-Uniform Horizontal Stress–Strain Distribution on the Mechanical Properties of Combinations

The deformation of primary coal-rock combinations under conventional triaxial stress conditions is illustrated in Figure 16. To clearly demonstrate such differences, the coal and rock deformations in Figure 16 are amplified; in practice, the deformation difference between coal and rock is not as distinct as that shown in Figure 16. When the model has equal horizontal principal stress directions with dimension *D*, the influence range of the interface in the vertical direction under conventional triaxial stress is approximately 48% of the interface dimensions of the primary coal-rock combinations, meaning that the vertical influence height is around 0.48$D$. For the coal-rock body within the influence range of the interface, the coal undergoes compressive stress due to interface constraints, while the rock experiences tensile stress due to interface expansion, resulting in an increase in coal strength and a decrease in rock strength. Based on the interface's influence on coal and rock stresses, the coal body within a distance of 0.48$D$ from the interface is defined as the high-confining-pressure zone, the rock body within 0.48$D$ from the interface is defined as the low-confining-pressure zone, and the coal-rock body beyond a distance of 0.48$D$ is defined as the original-confining-pressure zone.

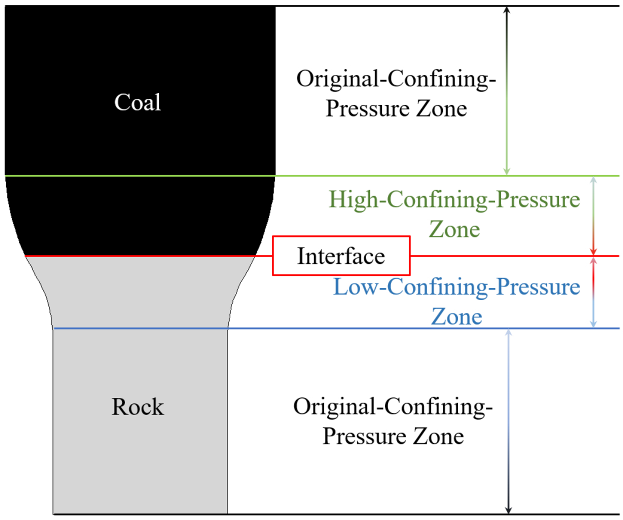


**Figure 16.** Horizontal stress distribution in primary coal-rock combination.

From the experimental results in Section 2, it is evident that the strength of primary coal-rock combinations is higher than that of coal specimens, and the strengths of these combinations decrease as the coal-rock ratio increases. This is attributed to the presence of the high-confining-pressure zone within the primary coal-rock combinations as compared with original coal, where the failure of the coal body within the combination requires a higher load and energy. For primary coal-rock combinations with the same lateral dimensions but different coal-rock height ratios, the range of the high-confining-pressure zone remains fixed. Changes in the coal-rock height ratio effectively alter the proportion of the high-confining-pressure zone within the coal body; as the coal proportion increases, the proportion of the high-confining-pressure zone in the coal body decreases, thus requiring less external load and energy for failure. Consequently, the strength of the primary coal-rock combination decreases, gradually approaching the strength of original coal as the coal proportion increases.

## 6. Conclusions

This study focused on primary coal-rock combinations, conducting experimental research, numerical simulations, and theoretical analyses to obtain the characteristics of their transverse mismatching deformation distribution. A model for the transverse mismatching deformation distribution of primary coal-rock combinations was established based on the Sigmoid function. The main conclusions are as follows:

(1) Differences in the mechanical parameters of coal and rock and constraints at the coal-rock interface can lead to mismatching horizontal deformation in coal-rock combinations. The relationship of the horizontal deformation magnitudes is coal > rock > interface. The horizontal deformation distribution of a primary coal-rock combination, which possesses cohesion between the layers, is continuous and smooth,

while the deformation of a coal-rock combination without cohesion exhibits a jump transition at the interface.

(2) The influence of interface constraints on horizontal deformation in coal and rock does not abruptly vanish as the distance from the interface increases; rather, it gradually diminishes to a negligible level, attenuating to an insignificant degree at approximately 48% of the model's lateral dimensions. The horizontal strain and stress distribution models for coal-rock combinations were established based on the Sigmoid function, with the $b$ value being 15.9, while the remaining parameters could be obtained through measurement or calculation.

(3) The mismatching deformation in coal and rock leads to the emergence of a high-confining-pressure zone within the coal body, resulting in enhanced strength of the coal body; thus, the strength of coal-rock combinations exceeds that of coal. When the lateral dimensions of the primary coal-rock combinations are fixed, the range of the high-confining-pressure zone remains constant. As the proportion of coal increases, the proportion of the high-confining-pressure zone within the coal body decreases, consequently reducing the strength of the primary coal-rock combinations as the coal-rock ratio increases.

**Author Contributions:** Methodology, investigation, formal analysis, data curation, writing—original draft, Q.F.; writing—review and editing, validation, supervision, investigation, data curation, funding acquisition, T.D.; writing—review and editing, resources, project administration, methodology, investigation, funding acquisition, Y.C.; writing—review and editing, validation, methodology, supervision, data curation, C.X.; writing—review and editing, formal analysis, funding acquisition, Z.Q.; data curation, formal analysis, R.S.; writing—review and editing, investigation, R.Y. All authors have read and agreed to the published version of the manuscript.

**Funding:** This research was supported financially by the "Tianchi Talents" Introduction Plan, the National Natural Science Foundation of China [grant number U23B2093, 52204220], the projects of Science and Technology Innovation and Entrepreneurship Fund of China Coal Science and Industry Group [grant number 2025-QRTC003].

**Data Availability Statement:** Data will be made available on request.

**Conflicts of Interest:** Authors Qiang Fu, Taotao Du, Zihan Qin and Ruda Sun were employed by the CCTEG and Tiandi Science and Technology Co., Ltd. Author Ruibing Yan was employed by the Xinjiang Energy and Chemical Industry Co., Ltd., CHN Energy. The remaining author declares that the research was conducted in the absence of any commercial or financial relationships that could be construed as a potential conflict of interest.

## References

1. Qin, T.; Song, Y.; Zhang, Y.; Duan, Y.W.; Liu, G. Study on mechanical response of composite rock mass with different coal seam dip angles under impact load. *Processes* **2026**, *14*, 738. [CrossRef]
2. Xie, H.P.; Zhou, H.G.; Xue, D.J.; Wang, H.W.; Zhang, R.; Gao, F. Research and consideration on deep coal mining and critical mining depth. *J. China Coal Soc.* **2012**, *37*, 535–542. [CrossRef]
3. Zhang, J.; Wang, B.F.; Lv, Y.H.; Liu, X.Y. Fuzzy comprehensive evaluation of rock burst risk based on combined subjective and objective weighting. *Sci. Rep.* **2026**. [CrossRef] [PubMed]
4. Li, P.Y.; Zhang, Y.J.; Zhang, L.Y.; Kong, J.Y. Research on the response mechanism of overlying strata failure and ground fissures development under high-intensity mining. *Processes* **2026**, *14*, 565. [CrossRef]
5. Li, Z.Y.; Zhao, G.M.; Cheng, X.; Qing, Z.H.; Meng, X.R.; Wu, X.K. Influence of loading system stiffness on failure mode and energy evolution law of coal-rock combination. *Eng. Fail. Anal.* **2026**, *185*, 110427. [CrossRef]
6. Li, X.P.; Li, H.T.; Zhang, X.F.; Yuan, H.H.; Li, X.S.; Shi, C.H.; Zheng, J.W.; Yang, G.Y.; Zhang, L.; Lei, G.R. Damage evolution of coal with a strong bursting liability and 3D measurement method for elastic deformation energy distribution. *Theor. Appl. Fract. Mech.* **2024**, *133*, 104534. [CrossRef]

7. Yuan, L. Strategic thinking of simultaneous exploitation of coal and gas in deep mining. *J. China Coal Soc.* **2016**, *41*, 1–6. [CrossRef]
8. Wang, K.; Zou, X.H.; Du, F.; Sun, J.Z.; Zhang, X.; Li, K.N.; Ju, Y. Seepage-damage-failure of gas-bearing coal-rock composite system subjected to different conditions: Implication for disaster prevention mechanism of outburst-rockburst composite dynamic disaster. *Nat. Resour. Res.* **2026**, *35*, 2003–2045. [CrossRef]
9. Wang, K.; Du, F. Research progress and prospect on coal-rock-gas compound dynamic disaster mechanism. *Safety* **2022**, *43*, 1–10. [CrossRef]
10. Chen, G.B.; Wang, E.Y.; Wang, W.C.; Li, T.; Zhang, G.H. Experimental study on the influence of lithology and rock-coal height ratio on mechanical properties and impact effect of combined body. *Energy Sources Part A Recovery Util. Environ. Eff.* **2019**, *46*, 4257–4280. [CrossRef]
11. Cong, R.C.; Yang, R.Y.; Liu, Y.W.; Li, G.S.; Huang, Z.W.; Zhang, B. Influence of interfacial properties on mechanical behaviors and failure patterns of coal-measure thin interbedded rocks under uniaxial compression using 3D FDEM. *Rock Mech. Rock Eng.* **2025**, *58*, 3589–3610. [CrossRef]
12. Zhou, Z.L.; Chen, L.; Cai, X.; Shen, B.T.; Zhou, J.; Du, K. Experimental investigation of the progressive failure of multiple pillar-roof system. *Rock Mech. Rock Eng.* **2018**, *51*, 1629–1636. [CrossRef]
13. Gong, F.Q.; Ye, H.; Yong, L. Rate effect on the burst tendency of coal-rock combined body under low loading rate range. *J. China Coal Soc.* **2017**, *42*, 2852–2860. [CrossRef]
14. Yang, K.; Liu, W.J.; Dou, L.T.; Chi, X.L.; Wei, Z.; Fu, Q. Experimental investigation into interface effect and progressive instability of coal-rock combined specimen. *J. China Coal Soc.* **2020**, *45*, 1691–1700. [CrossRef]
15. Zhao, P.X.; He, Y.C.; Li, S.G.; Lin, H.F.; Jia, Y.Y.; Yang, E.H. Coal thickness effect on mechanics and energy characteristics of coal-rock combination model. *J. Min. Saf. Eng.* **2020**, *37*, 1067–1076. [CrossRef]
16. Chen, G.B.; Li, T.; Yang, L.; Zhang, G.H.; Li, J.W.; Dong, H.J. Mechanical properties and failure mechanism of combined bodies with different coal-rock ratios and combinations. *J. Min. Strat. Control Eng.* **2021**, *3*, 84–94. [CrossRef]
17. Liu, X.S.; Tan, Y.L.; Ning, J.G.; Lu, Y.W.; Gu, Q.H. Mechanical properties and damage constitutive model of coal in coal-rock combined body. *Int. J. Rock Mech. Min. Sci.* **2018**, *110*, 140–150. [CrossRef]
18. Yin, D.W.; Chen, S.J.; Sun, X.Z.; Jiang, N. Strength characteristics of roof rock-coal composite samples with different height ratios under uniaxial loading. *Arch. Min. Sci.* **2019**, *64*, 307–319. [CrossRef]
19. Zhao, T.B.; Gu, X.B.; Guo, W.Y.; Gong, X.F.; Xiao, Y.X.; Kong, B.; Zhang, C.G. Influence of rock strength on the mechanical behavior and P-velocity evolution of coal-rock combination specimen. *J. Mater. Res. Technol.* **2021**, *12*, 1113–1124. [CrossRef]
20. Zuo, J.P.; Chen, Y.; Cui, F. Investigation on mechanical properties and rock burst tendency of different coal-rock combined bodies. *J. China Univ. Min. Technol.* **2018**, *47*, 81–87. [CrossRef]
21. Guo, D.M.; Zuo, J.P.; Zhang, Y.; Yang, R.S. Research on strength and failure mechanism of deep coal-rock combination bodies of different inclined angles. *Rock Soil Mech.* **2011**, *32*, 1333–1339. [CrossRef]
22. Shen, W.B.; Yu, W.J.; Pan, B. Rock mechanics test and failure characteristics of coal-rock combination with different dip angles. *Min. Eng. Res.* **2021**, *36*, 1–8. [CrossRef]
23. Tien, Y.M.; Kuo, M.C.; Juang, C.H. An experimental investigation of the failure mechanism of simulated transversely isotropic rocks. *Int. J. Rock Mech. Min. Sci.* **2006**, *43*, 1163–1181. [CrossRef]
24. Wu, Y.P.; Yan, Z.Z.; Luo, S.H.; Tang, Y.P.; Wang, T.; Cao, J.L. Dip effect of stress transfer and structural instability mechanism of coal-rock combination. *Coal Sci. Technol.* **2023**, *51*, 105–116. [CrossRef]
25. Zhao, H.L.; Zhao, Y. Influence of dip angle of coal and rock combination on outburst tendency based on particle flow code. *Saf. Coal Mines* **2018**, *49*, 198–201. [CrossRef]
26. Song, H.Q.; Zuo, J.P.; Liu, H.Y.; Zuo, S.H. The strength characteristics and progressive failure mechanism of soft rock-coal combination samples with consideration given to interface effects. *Int. J. Rock Mech. Min.* **2021**, *138*, 104593. [CrossRef]
27. Xiong, H.X.; Wu, H.; Yang, Y.J.; Xia, Q.Y. Analysis of mechanical properties and failure characteristics of inclined coal-rock composites considering the prefabricated crack size. *Theor. Appl. Fract. Mech.* **2025**, *139*, 105114. [CrossRef]
28. Zheng, J.W.; Wang, S.W.; Li, H.T.; Yang, G.Q.; Lü, D.Z.; Liu, B.; Fu, Y.K.; Li, X.P.; Lei, G.R. Experimental study on compressive strength characteristics of coal-rock combinations influenced by number of bedding surfaces. *Coal Geol. Explor.* **2023**, *51*, 11–22. [CrossRef]
29. Xu, C.; Yang, T.; Wang, K.; Yuan, Y.W.; Guo, L. Influence of primary interface characteristics on mechanical properties and damage evolution of coal-rock combination. *Eng. Fail. Anal.* **2024**, *164*, 108658. [CrossRef]
30. Zhao, Z.; Wang, W.; Wang, L.; Dai, C. Compression-shear strength criterion of coal-rock combination model considering interface effect. *Tunn. Undergr. Space Technol.* **2015**, *47*, 193–199. [CrossRef]

31. Li, C.J.; Xu, Y.; Feng, M.M.; Pan, B. Deformation law and failure mechanism of coal-rock-like combined body under uniaxial loading. *J. China Coal Soc.* **2020**, *45*, 1773–1782. [CrossRef]
32. Cai, Y.B. Damage Induced Permeability Evolution in Stressed and Gas-Bearing Primary Coal-Rock Combination and Its Application. Doctoral Dissertation, China University of Mining and Technology, Beijing, China, 2021.